Study On Photocatalytic And Antibacterial Ability Of TiO_2 And TiO_2-SiO_2 Coatings

Kieu Do Trung Kien[1,2,*], Do Quang Minh[1,2], Huynh Ngoc Minh[1,2], and Nguyen Vu Uyen Nhi[1,2]

[1] *Department of Silicate Materials, Faculty of Materials Technology, Ho Chi Minh City University of Technology (HCMUT), 268 Ly Thuong Kiet Street, Ward 14, District 10, Ho Chi Minh City, Vietnam*
[2] *Vietnam National University Ho Chi Minh City, Linh Trung Ward, Thu Duc City, Ho Chi Minh City, Vietnam*
[*] *Corresponding author. E-mail: kieudotrungkien@hcmut.edu.vn*

Received: Feb. 07, 2024; Accepted: Apr. 01, 2024

Materials exhibiting photocatalytic properties have garnered considerable attention for diverse applications, including degrading toxic organic compounds, disinfection, and developing self-cleaning surfaces. This study focuses on the synthesis of coatings based on TiO_2 and TiO_2-SiO_2, accomplished through the sol–gel method using Tetra-n-butyl ortho titanate and Tetraethyl orthosilicate precursors, followed by calcination at 500 °C. The phase compositions of the resulting coatings were assessed using Fourier transform infrared spectroscopy (FTIR) and X-ray diffraction (XRD). The band gap energy was quantified through UV-Vis spectroscopy. The photocatalytic efficacy was examined by assessing the inhibition of Escherichia coli bacteria and the decomposition of the methylene blue solution. The adhesive capability of the coating to the ceramic tile substrate was evaluated via scanning electron microscopy. The outcomes reveal that the primary phase components of the coatings consist of anatase and rutile. The introduction of SiO_2 in conjunction with TiO_2 demonstrates a mitigating effect on the photocatalytic performance and organic matter decomposition compared to pure TiO_2. Nevertheless, this reduction is marginal, and SiO_2 positively influences enhancing the adhesion of the TiO_2 coating to the ceramic substrate material.

Keywords: TiO_2; TiO_2-SiO_2; photocatalyst; antimicrobial application

http://dx.doi.org/10.6180/jase.202503_28(3).0004

1. Introduction

TiO_2 is a semiconductor characterized by a wide band gap and transparency, rendering it a staple in various industries, including wall paint, paper, pigments, cosmetics, etc. Beyond its conventional applications, TiO_2 possesses noteworthy photochemical and super-hydrolysable properties at the nanoscale [1]. The photochemical attributes of TiO_2 were initially unveiled by Fujishima [2] in the late 1960s, and in 1995, Sakai et al. [3] further discovered the phenomenon of super hydrolysis, unlocking critical applications. Such robust redox characteristics endow TiO_2 with versatility across various domains. TiO_2 plays a role in the sustainable degradation of hazardous substances, including toxic organic compounds, viruses, and bacteria [4]. TiO_2 exists in three allotropes: Anatase, brookite, and rutile [5]. Anatase and Rutile are the most prevalent among these. Anatase is renowned for its photocatalytic attributes, particularly under UV ultraviolet radiation. Rutile is commonly employed in producing refractory ceramics, pigments, and other applications [6–8]. Rutile powder is a whitening agent in paper, plastic, paints, and glazes [9–11].

Due to its photochemical capabilities, TiO_2 is an advantageous coating for enhancing the surface properties of various materials. Beyond its photochemical attributes,

TiO_2 coatings also exhibit a pronounced superhydrophobic effect [12]. This effect imparts self-cleaning properties to surfaces coated with TiO_2. When applied as a coating for ceramic glaze, TiO_2 plays a crucial role in preventing fading caused by rainwater. This underscores the potential of TiO_2 coatings, particularly in ceramic glaze. TiO_2-coated ceramic glazes maintain their color integrity and boast self-sterilizing and self-cleaning capabilities, owing to the combined influence of their photochemical properties and super-wetting characteristics.

Nevertheless, TiO_2 coatings often exhibit poor surface bonding, leading to peeling and a subsequent loss of photocatalytic efficacy over time. Addressing this challenge, numerous studies have sought to enhance the adhesive properties of TiO_2 on substrates. Zhang and Lei [13] investigated the amalgamation of TiO_2 and Fe_2O_3 to augment adhesion to metal surfaces. Results indicate that the TiO_2-Fe_2O_3 film adheres effectively to metal surfaces without significantly compromising the photocatalytic prowess of TiO_2. With a plastic substrate, Neti and Joshi [14] blended TiO_2 with cellulose and applied it as a coating on an acrylic plastic base. The findings similarly indicate improved adhesion between the coating and the substrate while retaining TiO_2 properties. Kien et al. [15] combined TiO_2 with the Bi_2O_3-B_2O_3-ZnO glass system to pursue enhanced coating adhesion. This resultant coating system possesses a low melting temperature, facilitating robust bonding with the glass substrate while maintaining photocatalytic and bactericidal properties.

In the present study, TiO_2 and TiO_2-SiO_2 coatings were synthesized using TiO_2 and SiO_2 sols. Fourier Transform Infrared Spectroscopy and X-ray diffraction methods were employed to assess the resulting coating's functional group composition and phase composition. The coating's ability to bond with the ceramic substrate was examined through scanning electron microscopy. The photocatalytic and bactericidal capacities were evaluated by assessing the coating's capability to decolorize methylene blue solution and combat Escherichia coli bacteria on agar plates. Numerous studies have been conducted on the photocatalytic properties of TiO_2 and the combination of TiO_2-SiO_2. However, within the context of our research, there has been no investigation into the properties of TiO_2 and TiO_2-SiO_2 synthesized from TiO_2 and SiO_2 sols at 500 °C. This temperature coincides with the softening range of the tile glaze, making it suitable for coating TiO_2 and TiO_2-SiO_2 onto tile surfaces.

2. Experimental procedures

2.1. Materials and experimental diagram

TiO_2 and TiO_2-SiO_2 coatings were formulated using TiO_2 and SiO_2 sols. The TiO_2 sol was synthesized from Tetra-n-butyl orthotitanate ($Ti(OCH(CH_3)_2)_4$), while the SiO_2 sol was synthesized from Tetraethyl orthosilicate ($Si(OC_2H_6)_4$). The sol synthesis process for TiO_2 and SiO_2 followed the procedures outlined in the Kien et al. [16]. All chemicals used in the study were procured from Merck. The specimen exclusively employing TiO_2 sol was denoted as T100. The specimen incorporating 90% TiO_2 sol and 10% SiO_2 sol was labeled T90. The properties and adhesion of TiO_2 and TiO_2-SiO_2 coatings to ceramic tile substrates were subsequently analyzed, as illustrated in Fig. 1.

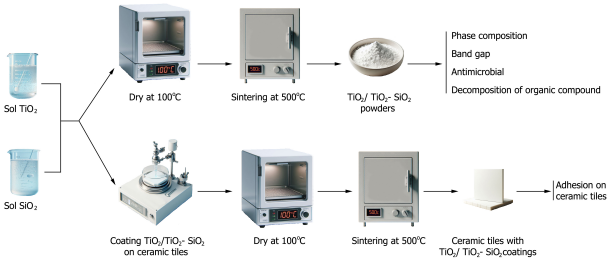

Fig. 1. A diagram of the prototyping process

TiO_2 and SiO_2 sols were dried at 100 °C and calcined at 500 °C to produce TiO_2 and TiO_2-SiO_2 coatings. The resulting sintered product was finely powdered and subjected to X-ray diffraction and Fourier infrared transform analyses to assess mineral composition and functional groups. The coatings' band gap energy was determined utilizing the UV-Vis method. The ability to decompose organic matter was evaluated through methylene blue solution decomposition, while antibacterial efficacy was assessed by inhibiting Escherichia coli bacteria on agar plates. The adhesion capabilities of TiO_2 and TiO_2-SiO_2 coatings were investigated by applying them to the surfaces of ceramic tiles measuring 50 x 50 mm. Subsequently, the tiles underwent drying at 100 °C followed by sintering at 500 °C. The adhesion of the coating post-sintering was examined using a scanning electron microscope.

2.2. Determine function groups

The functional group composition of the TiO_2-SiO_2 coating after sintering at 500 °C was assessed using the Fourier transform infrared (FTIR) method. Functional groups are crucial in evaluating coating formation and adhesion to the ceramic substrate. The FTIR analysis used a Bruker–Tensor 37 instrument with KBr as the binder. The scanning fre-

quency was set at 10 kHz, spanning the range from 4000 to 300 cm^{-1} and employing a scanning step of 0.96 cm^{-1}.

2.3. Determine phase compositions

X-ray diffraction (XRD) analysis was employed to determine the mineral composition. The XRD analysis utilized a Bruker–D8 Advance instrument with Cu_{α} radiation (1.54184Å). The analytical range spanned from 20 to 80°, with a scan step of 0.02°. The resulting phase composition was calculated based on the XRD patterns, employing Eq. (1) for this purpose.

$$\%C = \frac{s_C}{\sum s} \quad (1)$$

The Eq. (1) provided calculates the percentage of crystals (%C), where %C is determined by the ratio of the crystalline area to be calculated (S_c) to the total crystalline area (ΣS).

2.4. Determine the band gap energy

The band gap energy of the TiO_2-SiO_2 coating was determined using the UV-Vis method. The UV-Vis analyzer employed for this purpose was Jssco V550 UV/VIS. The relationship between the absorption coefficient (α) and the band gap energy $\left(Eg_g\right)$ is expressed by Eq. (2) [17, 18].

$$(\text{ahv})^m = \text{B}\left(hv - E_g\right) \sim f(E) \quad (2)$$

$$\text{a} = \frac{2.303\ \text{A}}{l} \quad (3)$$

Where a is molar absorptivity and calculated according to Eq. (3). A is constant, h is Planck's constant, v is the frequency of light, λ is the wavelength of light, E_g is band gap energy, c is the speed of light, $l = 1$ is is the thickness of the sample, and the exponent $m = 1/2$ [19, 20].

2.5. Determine to decompose organic matter ability

The assessment of the organic matter decomposition was conducted by examining the decolorization of methylene blue trihydrate ($C_{16}H_{18}ClN_3S{\cdot}3H_2O$ – MB). MB solution is known for absorbing characteristic light at a wavelength of 664 nm. The extent of light absorption at 664 nm is directly correlated with the concentration of MB solution. Hence, the concentration of MB in the solution can be accurately determined by measuring its light absorption at 664 nm. UV-Vis spectroscopy is commonly employed for this purpose.

A quantity of 25 mg of TiO_2-SiO_2 powder was dispersed in 10 mL of a BM solution with a concentration of 50 mg/L. The mixture was subjected to illumination under a 40 W compact lamp with a light wavelength ranging from 400 to 600 nm. Samples were illuminated at 1, 5, 10, 20, and 30 hours. The concentration of the MB solution after different digestion times was determined using the UV-VIS spectrum.

2.6. Determine antibacterial ability

The antibacterial capability was assessed by inhibiting the growth of *Escherichia coli* (*E. coli*) bacteria. If a compound can inhibit the growth of *E. coli* bacteria, it is likely to exhibit similar inhibitory effects on other gram-negative bacteria. The antibacterial testing steps for *E. coli* are conducted in accordance with ISO 20776-1:2006 standards and are summarized briefly as follows:

- Prepare *E. coli* ATCC 25922 Bacteria: Follow established standards to prepare a culture of *E. coli* ATCC 25922 bacteria. This strain is commonly used as a reference in microbiology.

- Prepare Antibacterial Solution: Create a solution containing antibacterial substances at two different concentrations: 310 μg/mL and 160 μg/mL.

- Prepare Agar Plates: Mix Mueller-Hinton agar plates with solutions containing TiO_2 (titanium dioxide) and TiO_2-SiO_2 (titanium dioxide-silicon dioxide).

- Inoculate Bacteria: Place the prepared *E. coli* bacteria onto the agar plates.

- Incubate: Incubate the agar plates at 37 °C for 20 hours. Maintain continuous compact fluorescent lighting during incubation.

- Observe Growth: After incubation, check and observe the growth of *E. coli* bacteria in the test samples.

2.7. Determine to bond with ceramic tile substrate ability

The adhesion of the coating to the surface was assessed using the scanning electron microscope (SEM) method. The analysis was conducted using a Hitachi – S4800 microscope at a voltage of 10 kV, with a magnification of 300 times.

3. Result and discussions

3.1. Functional group composition

After sintering at 500 °C, the structural analysis of the mixtures was conducted using the FTIR method. Fig. 2 illustrates the FTIR analysis results for samples with and without SiO_2. In the T100 sample, representing the component without SiO_2, vibrations were observed at wavenumbers 3235, 2345, 1636, 648, and 625 cm^{-1}. In the T90 sample, corresponding to 10% TiO_2 sol, vibrations were detected at wavenumbers 3425, 1629, 1059, 928, 649, and 622 cm^{-1} [21–23].

The FTIR spectrum indicates the formation of Ti-O-Ti bonds in both samples, which are characteristic bonds of TiO_2 formed after sintering at 500 °C. In the T90 sample, in addition to the TiO_2 bonds, $Si-O-Si$ and $Ti-O-Si$ bonds are also evident. The $Ti-O-Si$ bonding appears when SiO_2 sol and TiO_2 sol are sintered at 500 °C, forming a bond between Ti and Si through an oxygen bridge.

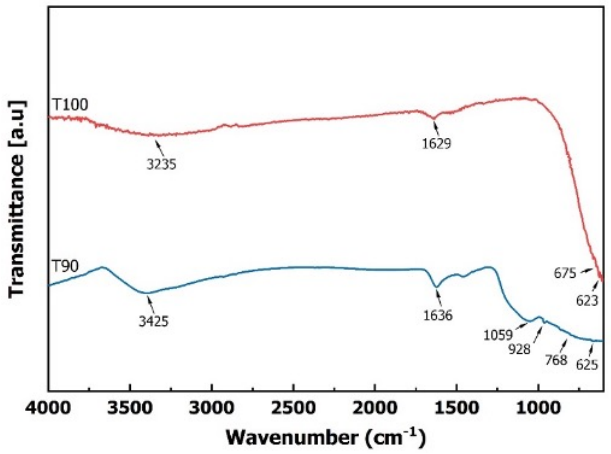

Fig. 2. The FTIR spectrum of TiO_2 (T100) and TiO_2-SiO_2 (T90) coatings

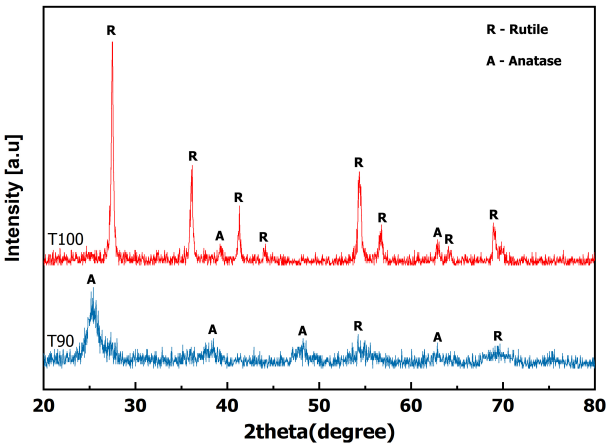

Fig. 3. The XRD patterns of TiO_2 (T100) and TiO_2-SiO_2 (T90) coatings

This bonding type can potentially enhance the adhesion between the TiO_2 coating and the substrate, particularly ceramic substrates based on $[SiO_4]^{4-}$ [24]. The $Si-O-Si$ bond is characteristic of SiO_2 and was formed after the dehydration of silica sol. This bond suggests that SiO_2 was not entirely consumed in the reaction to create $Ti-O-Si$ bonds but remains as free SiO_2. In addition to the mentioned bonds, $Ti-OH$, $Si-OH$, and $-OH$ represent physical and chemical water present in the samples.

3.2. Mineral composition

Fig. 3 presents the outcomes of the XRD patterns. The patterns reveal the presence of rutile and anatase minerals in both T100 and T90 samples. Rutile (R060745) exhibits diffraction peaks at 37.34°, 36.20°, 41.15°, 44.07°, 54.86°, 64.52°, and 69.12° [25, 26]. Anatase (R060277) exhibits diffraction peaks at 25.22°, 38.43°, 47.85°, and 62.63° [16, 26]. Anatase is initially formed and subsequently converted to rutile under the influence of temperature [27]. The FTIR results of the T90 sample suggest an incomplete reaction and the presence of SiO_2 in a free form. However, the XRD pattern of the T90 sample does not display characteristic peaks of SiO_2 crystals such as quartz, cristobalite, and tridymite. This observation confirms the existence of residual SiO_2 in an amorphous state. The amorphous form of SiO_2, as evidenced by the XRD pattern of sample T90, may impede the allotropic conversion of anatase to rutile. The XRD results reveal the presence of only rutile and anatase minerals in the samples, which indicates a favorable reaction efficiency during the creation of TiO_2. The heating process of the sol-gel mixture appears to be quite effective in producing titanium dioxide.

The hindrance of the allotropy transformation process from anatase to rutile by amorphous SiO_2 is further elucidated by calculating the crystalline content using Eq. (1) and the XRD patterns in Fig. 3. The results indicate that the T100 sample comprises 3.48% anatase and 96.52% rutile by weight. In contrast, the T90 sample includes 68.79% anatase and 31.21% rutile by weight. Using SiO_2 sol impeded the allotropy transformation of TiO_2 from anatase to rutile during heating. The reason may be that part of the heat energy is lost due to the allotropic transformation of the SiO_2. Previous research has demonstrated that anatase exhibits superior photocatalytic and bactericidal capabilities compared to rutile [28]. Therefore, the presence of anatase minerals in the TiO_2-SiO_2 coating has the potential to enhance its photocatalytic and antibacterial properties. The photocatalytic ability of the samples was assessed through the UV-Vis method.

3.3. Band gap energy

Fig. 4 displays the UV-Vis spectrum of the T90 and T100 samples. The absorption spectrum results reveal varying absorption capacities of the samples across different wavelength ranges. In the 200 to 350 nm wavelength range, the T90 sample exhibits higher light absorption than the T100 sample. Conversely, in the range from 350 to 800 nm, the T100 sample demonstrates superior absorption compared to the T90 sample. The light absorption capability could also help assess a material's photocatalytic potential. Based on these findings, it can be inferred that within the 350 - 800 nm range, the T100 sample, devoid of SiO_2, is more efficiently excited by light than the T90 sample. This wavelength range encompasses visible light (380 - 760 nm), indicating that coatings containing To further elucidate the photocatalytic ability, the band gap energy of the samples

was computed using Eqs. (2) and (3)

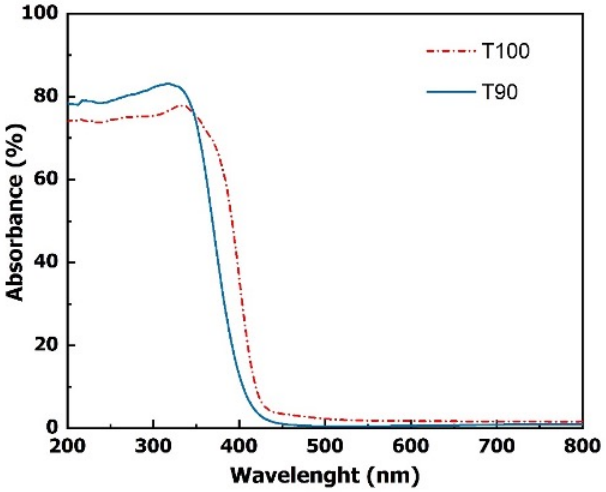

Fig. 4. The UV-Vis spectrum of the T90 and T100 samples

Fig. 5 illustrates a graph determining the band gap energy of the samples. The discrete form of the calculated points shows that these points can be expressed as changing values according to the rules of the Edgeworth - Cramer equation. Solving the second derivative equations identifies inflection points on the graph of Fig. 5, yielding values of 3.24 eV and 3.06 eV, respectively. The intersection of the tangent lines and the coordinate axis at the inflection point provides the band gap energy values for the T90 and T100 samples. The determined band gap energy for the T90 sample is 2.88 eV (corresponding to a wavelength of 430 nm), while that for the T100 sample is 2.84 eV (corresponding to a wavelength of 436 nm). These results indicate that both coating samples possess photocatalytic ability in the visible light range. The increased band gap energy of the T90 sample is attributed to the presence of SiO_2, which itself has a large band gap energy ($\sim$ 10 eV). The presence of SiO_2 elevates the coating's band gap energy, but it doesn't significantly impede the photocatalytic ability, as SiO_2 also hinders the allotropy transformation from anatase to rutile. The presence of SiO_2 with the appropriate composition has minimal impact on the coating's photocatalytic ability, as further corroborated by investigations into the ability to decompose organic compounds and the antibacterial properties of the T90 and T100 samples.

3.4. Ability to decompose organic compounds

The antibacterial ability was assessed by examining the inhibitory effect on Escherichia coli bacteria on an agar plate with 310 and 160 μg/mL bacterial concentrations. Fig. 6 depicts that all samples exhibited no evidence of *Escherichia coli* bacterial clusters forming after 20 hours of

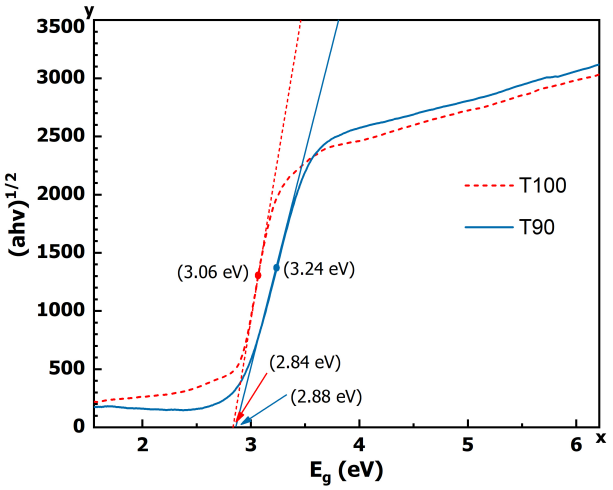

Fig. 5. Band gap analysis using UV-Vis spectrum

incubation at 37 °C. The antibacterial effect has been convincingly demonstrated through experiments inhibiting the growth of *E. Coli* bacteria. These experiments were conducted following the ISO 20776-1:2006 standard, and the results indicate the absence of *E. Coli* bacteria under standard experimental conditions. These results demonstrate the antibacterial efficacy of the T90 and T100 samples at different bacterial concentrations. Both samples exhibited the capability to decompose bacteria and hinder their growth on agar plates.

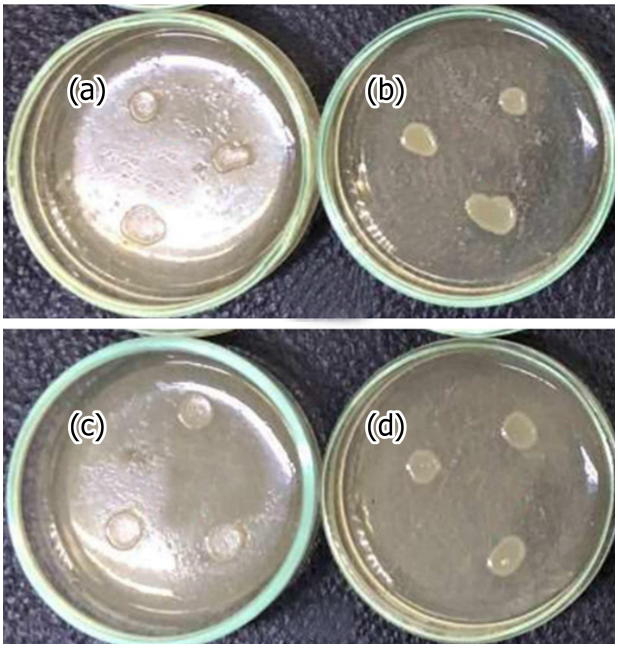

Fig. 6. (a) The T90 sample with a bacterial concentration of 310 μg/mL and (b) 160 μg/mL; (c) The T100 sample with a bacterial concentration of 310 μg/mL and (d) 160 μg/mL

Fig. 7 presents the color of the MB solution after reacting with the T100 and T90 samples at various soaking times. The MB decomposition experiment is a frequent assay for materials capable of decomposing organic compounds or functioning as adsorbents/absorbents. In this particular study, MB was used to assess the efficacy of TiO_2 and TiO_2-SiO_2 coatings in decomposing organic compounds. Effective decomposition of MB organic matter indicates the potential of these coatings to treat other organic compounds present in wastewater, provided they possess comparable durability. Observations from Fig. 7 reveal that, at equivalent time intervals, the color of the MB solution in the T100 sample is lighter than that in the T90 sample. The color of the MB solution serves as a visual indicator for assessing the concentration of the MB solution in the sample. This outcome partially evaluates the samples' ability to reduce organic compounds. The T100 sample demonstrated a more efficient decomposition of MB than the T90 sample. However, this difference is not significant.

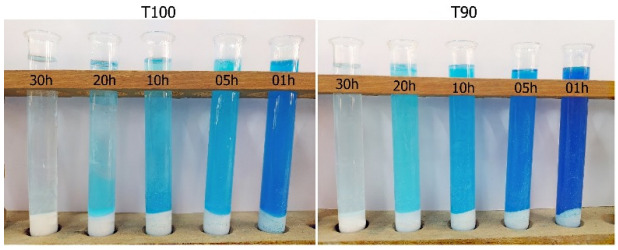

Fig. 7. Color change of MB solution

The ability to reduce MB in solution was quantified by determining the remaining MB content, and the results are depicted in Fig. 8. The decrease in remaining MB content with increasing soaking time indicates the samples' capacity to decompose MB. The findings consistently suggest that the T100 sample exhibited a better ability to decompose MB than the T90 sample at all soaking times. This alignment with the band gap energy calculation and the visual images in Fig. 6 suggests that the T100 sample, possessing a lower band gap energy, is better activated by visible light, leading to enhanced decomposition ability. However, it's worth noting that the difference in decomposition ability is most pronounced in the early periods (1 hour and 5 hours). The disparity in MB content becomes less significant for the 10, 20, and 30 hours intervals. The overall results suggest that the inclusion of SiO_2 sol in the mixture at a concentration of 10% (wt.) may diminish the TiO_2's ability to decompose MB, but this decrease is not significant.

In Figs. 4 and 5 the UV-Vis spectrum experiments have

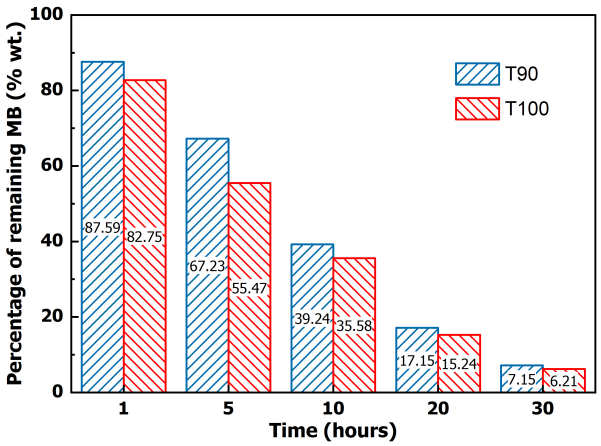

Fig. 8. The remaining percentage of MB solution after 1 – 30 hours

revealed that both TiO_2 and TiO_2-SiO_2 exhibit low band gap energies (2.84 eV and 2.88 eV). This low band gap energy can be attributed to the nanoscale existence of TiO_2, a phenomenon previously highlighted by various research groups [29, 30]. Importantly, this property enables the synthesized coatings to be activated by visible light, allowing them to decompose organic compounds effectively and exhibit antibacterial properties. The slow degradation efficiency observed for MB compound in Figs. 7 and 8 (lasting more than 20 hours) is due to the relatively large concentration of the MB solution used in this experiment.

Waste organic compounds and gram-negative bacteria commonly coexist in wastewater. Consequently, TiO_2 and TiO_2-SiO_2 coatings can be practical materials for treating anaerobic bacteria and decomposing organic compounds in wastewater. In this study, TiO_2 and TiO_2-SiO_2 were coated onto the surfaces of ceramic materials to enhance their antibacterial capabilities. Ceramics coated with TiO_2 or TiO_2-SiO_2 can be used in environments that frequently encounter wastewater, such as bathrooms.

3.5. Ability to bond with ceramic tile substrate

Fig. 9 provides a photograph of the sample's surface after being coated with the TiO_2 and TiO_2-SiO_2 layers, along with an image of the microstructure at the contact point between the coating layer and the ceramic tile substrate. The photos illustrate that the TiO_2 and TiO_2-SiO_2 coatings are uniformly distributed on the tile surface. The tile surface does not exhibit clustered glaze spots, and there are no cracks on the glaze surface. Moreover, there is no evidence of warping in the tile, indicating that the thermal expansion coefficient of the coating is compatible with the glaze surface and ceramic substrate. These results suggest

TiO_2 and TiO_2-SiO_2 coatings adhere well to the glaze surface. Consequently, TiO_2 and TiO_2-SiO_2 coatings could be effectively employed as antibacterial coatings for ceramic tiles

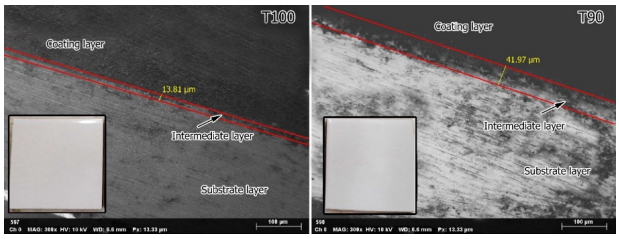

Fig. 9. Cross-sectional microstructure image at the contact position between the coating and the ceramic substrate

The scanning electron microscope (SEM) image at the contact surface between the ceramic substrate and the coating at 300 times magnification provides their bonding ability. The SEM image in Fig. 9 reveals two distinct regions in both T90 and T100 samples. The dark-colored area represents the location of the TiO_2 and TiO_2-SiO_2 coating, while the light-colored area corresponds to the ceramic substrate. The intermediate region between these two layers is marked with a red line. Measuring the thickness of the intermediate layer on SEM images indicates that the T90 sample has a thickness of 41.97 μm, while the T100 sample has a thickness of 13.81 µm. These results suggest that incorporating SiO_2 may have diminished the photocatalytic and antibacterial properties of the coating. However, it has resulted in a more robust bond with the ceramic substrate, leading to a coating with improved durability and adhesion to the ceramic substrate.

4. Conclusions

The study on TiO_2 and TiO_2-SiO_2 coatings, fabricated from TiO_2 and SiO_2 sols at a sintered temperature of 500 °C, yields several key conclusions:

- *Functional Group Composition Analysis*: The analysis of functional group composition revealed characteristic $Ti-O$ bonds in all samples, indicating the formation of TiO_2. Samples containing SiO_2 also exhibited Ti - O - Si bonds, potentially enhancing the adhesion of the coating to the ceramic substrate.

- *Phase Composition Analysis*: Phase composition analysis shows rutile and anatase as the main mineral components in the samples. Samples with SiO_2 displayed a higher content of anatase compared to rutile. Increased anatase content could contribute to improved photocatalytic and antibacterial properties of the coating.

- *Band Gap Energy Determination*: The band gap energy determination results indicated that the TiO_2 sample had a lower band gap energy (2.84 eV) than the TiO_2-SiO_2 sample (2.88 eV). This minor difference suggests that the addition of SiO_2 has minimal impact on the photocatalytic ability of the coating.

- *Antibacterial and Decomposition Ability*: Antibacterial ability assessments demonstrated that all samples effectively resisted *Escherichia coli* bacteria at concentrations of 310 and 160 μg/mL for 20 hours at 37 °C. The ability to decompose methylene blue was slightly higher in the TiO_2 sample than in the TiO_2-SiO_2 sample, but the difference was insignificant.

- *Coating Durability and Adhesion*: Surface coating results on ceramic tiles revealed that both coatings could be applied successfully. However, the sample with SiO_2 exhibited better adhesion to the ceramic substrate than the sample with only TiO_2. Therefore, adding SiO_2 to the TiO_2 coating enhanced its durability with the ceramic substrate without significantly compromising its photocatalytic and antibacterial properties.

The study suggests that the TiO_2-SiO_2 coating balances durability and functional properties, making it a promising option for applications requiring both adhesion strength and photocatalytic/antibacterial performance.

5. Acknowledgements

We acknowledge the Ho Chi Minh City University of Technology (HCMUT), VNU – HCM for supporting this study.

References

[1] S. Saini, P. Basera, M. Kumar, P. Bhumla, and S. Bhattacharya, (2020) *"Metastability triggered reactivity in clusters at realistic conditions: a case study of N-doped (TiO2) n for photocatalysis"* **Journal of Physics: Materials 4**(1): 015001.

[2] A. Fujishima, (1969) *"Photosensitized electrolytic oxidation on semiconducting n-type TiO_2 electrode"* **Kogyo Kagaku Zasshi 72**: 108–113.

[3] H. Sakai, R. Baba, K. Hashimoto, A. Fujishima, and A. Heller, (1995) *"Local Detection of Photoelectrochemically Produced H2O2 with a" Wired" Horseradish Peroxidase Microsensor"* **The Journal of Physical Chemistry *99***(31): 11896–11900.

[4] A. Brindha and T. Sivakumar, (2017) *"Visible active N, S co-doped TiO2/graphene photocatalysts for the degradation of hazardous dyes"* **Journal of Photochemistry and Photobiology A: Chemistry *340***: 146–156.

[5] Y. Luo, A. Benali, L. Shulenburger, J. T. Krogel, O. Heinonen, and P. R. Kent, (2016) *"Phase stability of TiO2 polymorphs from diffusion Quantum Monte Carlo"* **New Journal of Physics *18***(11): 113049.

[6] X. Qi, L. Fu, R. Du, H. Gu, D. Chen, S. Yang, A. Huang, and R. Lv, (2023) *"Properties of various CaO-Al2O3-TiO2 refractories and their reaction behaviours in contact with Ti6Al4V melts"* **Journal of Alloys and Compounds *959***: 170599.

[7] J. George, C. Gopalakrishnan, P. Manikuttan, K. Mukesh, and S. Sreenish, (2021) *"Preparation of multipurpose TiO2 pigment with improved properties for coating applications"* **Powder technology *377***: 269–273.

[8] Y.-Q. Wang, L. Gu, Y.-G. Guo, H. Li, X.-Q. He, S. Tsukimoto, Y. Ikuhara, and L.-J. Wan, (2012) *"Rutile-TiO2 nanocoating for a high-rate Li4Ti5O12 anode of a lithium-ion battery"* **Journal of the American Chemical Society *134***(18): 7874–7879.

[9] A. E. Kabeel, R. Sathyamurthy, S. W. Sharshir, A. Muthumanokar, H. Panchal, N. Prakash, C. Prasad, S. Nandakumar, and M. El Kady, (2019) *"Effect of water depth on a novel absorber plate of pyramid solar still coated with TiO2 nano black paint"* **Journal of cleaner production *213***: 185–191.

[10] Y. Liang and H. Ding, (2020) *"Mineral-TiO2 composites: Preparation and application in papermaking, paints and plastics"* **Journal of Alloys and Compounds *844***: 156139.

[11] S. Teixeira and A. M. Bernardin, (2009) *"Development of TiO2 white glazes for ceramic tiles"* **Dyes and Pigments *80***(3): 292–296.

[12] Y. Yu, W. Cui, L. Song, Q. Liao, K. Ma, S. Zhong, H. Yue, and B. Liang, (2022) *"Design of organic-free superhydrophobic TiO2 with ultraviolet stability or ultraviolet-induced switchable wettability"* **ACS Applied Materials & Interfaces *14***(7): 9864–9872.

[13] X. Zhang and L. Lei, (2008) *"Preparation of photocatalytic Fe2O3–TiO2 coatings in one step by metal organic chemical vapor deposition"* **Applied Surface Science *254***(8): 2406–2412.

[14] N. R. Neti and P. Joshi, (2010) *"Cellulose reinforced-TiO 2 photocatalyst coating on acrylic plastic for degradation of reactive dyes"* **Journal of coatings technology and research *7***: 643–650.

[15] K. D. T. Kien, N. V. U. Nhi, H. N. Minh, and D. Q. Minh, (2022) *"Optical properties of the Bi2O3-B2O3-ZnO glass system combined with TiO2 or Ag/TiO2"* **Journal of Ceramic Processing Research *23***(3): 350–355.

[16] K. D. T. Kien, D. Q. Minh, H. N. Minh, and N. V. U. Nhi, (2023) *"SYNTHESIS OF TiO2–SiO2 FROM TETRA-N-BUTYL ORTHOTITANATE AND TETRAETHYL ORTHOSILICATE BY THE SOL-GEL METHOD APPLIED AS A COATING ON THE SURFACE OF CERAMICS"* **Ceramics–Silikáty *67***(1): 58–63.

[17] P. George and P. Chowdhury, (2019) *"Complex dielectric transformation of UV-vis diffuse reflectance spectra for estimating optical band-gap energies and materials classification"* **Analyst *144***(9): 3005–3012.

[18] Ö. B. Mergen and E. Arda, (2020) *"Determination of optical band gap energies of CS/MWCNT bionanocomposites by Tauc and ASF methods"* **Synthetic Metals *269***: 116539.

[19] O. Sallam, A. Madbouly, N. Elalaily, and F. Ezz-Eldin, (2020) *"Physical properties and radiation shielding parameters of bismuth borate glasses doped transition metals"* **Journal of Alloys and Compounds *843***: 156056.

[20] A. Agarwal, V. Seth, S. Sanghi, P. Gahlot, and D. Goyal, (2003) *"Optical band gap studies and estimation of two photon absorption coefficient in alkali bismuth borate glasses"* **Radiation effects and defects in solids *158***(11-12): 793–801.

[21] A. L. Smith, (1960) *"Infrared spectra-structure correlations for organosilicon compounds"* **Spectrochimica Acta *16***(1-2): 87–105.

[22] J. Ren, Z. Li, S. Liu, Y. Xing, and K. Xie, (2008) *"Silica–titania mixed oxides: Si–O–Ti connectivity, coordination of titanium, and surface acidic properties"* **Catalysis Letters *124***: 185–194.

[23] V. A. Zeitler and C. A. Brown, (1957) *"The Infrared Spectra of Some Ti-O-Si, Ti-O-Ti and Si-O-Si Compounds"* **The Journal of Physical Chemistry *61***(9): 1174–1177.

[24] A. Bronson and J. Chessa, (2008) *"An evaluation of vaporizing rates of SiO2 and TiO2 as protective coatings for ultrahigh temperature ceramic composites"* **Journal of the American Ceramic Society *91***(5): 1448–1452.

[25] K. D. T. Kien, N. V. U. Nhi, H. N. Minh, and D. Q. Minh, (2022) *"Optical properties of the Bi2O3-B2O3-ZnO glass system combined with TiO2 or Ag/TiO2"* **Journal of Ceramic Processing Research *23***(3): 350–355.

[26] C. Byrne, S. Rhatigan, D. Hermosilla, N. Merayo, Á. Blanco, M. C. Michel, S. Hinder, M. Nolan, and S. C. Pillai, (2019) *"Modification of TiO2 with hBN: high temperature anatase phase stabilisation and photocatalytic degradation of 1, 4-dioxane"* **Journal of Physics: Materials *3***(1): 015009.

[27] S.-J. Kim and K. Ogino, (2019) *"Synthesis of TiO2 nanoparticles using titanium tetraisopropoxide and starch"* **Journal of Ceramic Processing Research *20***(6): 665–669.

[28] J. ZHANG, Y. Song, F. Lu, W. Fei, Y. Mengqiong, L. Genxiang, X. Qian, W. Xiang, and L. Can, (2011) *"Photocatalytic degradation of rhodamine B on anatase, rutile, and brookite TiO2"* **Chinese Journal of Catalysis *32***(6-8): 983–991.

[29] B. Avinash, V. Chaturmukha, H. Jayanna, C. Naveen, M. Rajeeva, B. Harish, S. Suresh, and A. R. Lamani. "Effect of particle size on band gap and DC electrical conductivity of TiO2 nanomaterial". In: *AIP conference proceedings*. ***1728***. 1. AIP Publishing. 2016.

[30] R. Mechiakh, N. B. Sedrine, R. Chtourou, and R. Bensaha, (2010) *"Correlation between microstructure and optical properties of nano-crystalline TiO2 thin films prepared by sol–gel dip coating"* **Applied Surface Science *257***(3): 670–676.